ANALYSIS OF FORCE DYNAMICS FOR AIRFOIL IN THE WAKE OF DIFFERENT GRIDS

Muhammad Ramzan Luhur*, Abdul Latif Manganhar**, Shahid Hussain Siyal***, Khalid Hussain Solangi****

ABSTRACT

This paper presents the lift and drag force dynamics for an airfoil FX 79-W-151A under turbulent wind inflows generated with fractal and classical square grids. The force measurements were performed in a wind tunnel in the wake of these grids. The measured force dynamics is analyzed using classical averaging procedure and a Langevin approach. The comparison of lift and drag dynamics achieved in the wake of fractal and classical square grids, suggests that the fractal square grid contributes significantly extended lift and drag dynamics in terms of standard deviation from the mean as well as short-time local dynamics extracted by Langevin approach. Even at low turbulence level, the fractal square grid wake contributes much higher force fluctuations than the classical square grids.

Key words: *Wind tunnel measurements, force dynamics, airfoil, turbulent inflows, fractal square grid, classical square grid.*

1. INTRODUCTION

Wind turbines operate in dynamic wind fields, which contribute dynamic forces on wind turbine rotor blades. These blades are designed using airfoils that are commonly characterized by static lift and drag forces at fix angles of attack (AOAs) under steady low-turbulence flow [1, 2, 3]. However, in reality, most of the time, wind turbines encounter turbulent inflows due to ground boundary layer effects [4, 5, 6]. The turbulent inflows cause fast variations in AOA [7], which result substantial enlargement in lift and well-known dynamic stall effect [8, 9, 10], leading to large and rapid changing forces on the airfoil.

In order to investigate the dynamic behavior of forces on airfoils, different grids are designed to generate multi-scale turbulent inflows in wind tunnels. These mainly include the classical grids [11, 12, 13] and the fractal grids [14]. Recently, a type of an active grid has also been reported for multi-scale turbulence generation [15]. The classical grids use rectangular arrays of bars and fractal grids use geometric patterns repeated at smaller scales. The type of fractal square grid is experienced to generate more similar wind fluctuations to atmospheric wind than the classical grids [16, 17]. The fractal square grid produces small scale wind statistics similar to those observed in open-air [16].

The aim of this contribution is to provide insight on force dynamics achieved in the wake of fractal square grid and the classical square grids, in particular the comparison of local force fluctuations on short-time scales (high-frequency) obtained with these grids.

The paper is organized as follows. Section 2 describes the measurement details and the analysis approach applied. Section 3 presents the comparison of results from the described grids. The last Section 4 concludes the outcome.

2. METHODOLOGY

2.1. Experimental Data

The force measurements were performed in a wind tunnel for an airfoil FX 79-W-151A at University of Oldenburg Germany [16]. The airfoil was installed in vertical position in closed-loop test section of wind tunnel as shown in Figure 1. The test section has dimensions of 1 m wide, 0.8 m high and 2.6 m long. The mean wind inflow velocity was 50 m/s approximately. The airfoil chord length was 0.2 m leading to Reynolds number of $7x10^5$.

Figure 1: View of the wind tunnel test section. The black arrows indicate the installed position of strain gauge force sensors and the vertical airfoil [16].

* PhD researcher, ForWind-Centre for Wind Energy Research, University of Oldenburg, Germany.

** Assistant Professor, Quaid-e-Awam University of Engineering, Science and Technology, Nawabshah, Pakistan.

*** PhD Researcher, Royal Institute of Technology (KTH), Stockholm, Sweden.

**** PhD Researcher, University of Malaya, Kuala Lumpur, Malaysia.

The turbulent inflows were generated using fractal and classical square grids as shown in Figure 2. The used grids include; a 5-cm square mesh grid, a 10-cm square mesh grid and a fractal square grid yielding the turbulence intensity of 3.6%, 6.7% and 4.6%, respectively. The turbulence intensity is estimated using the relation.

$$T_i = \frac{\sigma_u}{\overline{u}} \tag{1}$$

Where $\overline{u}$ is the mean wind inflow and σ_u the standard deviation of wind inflow. All three (two different mesh size classical square grids of type as shown in Figure 2(a) and one fractal square grid as shown in Figure 2(b)) grids had a blockage ratio of 25%.

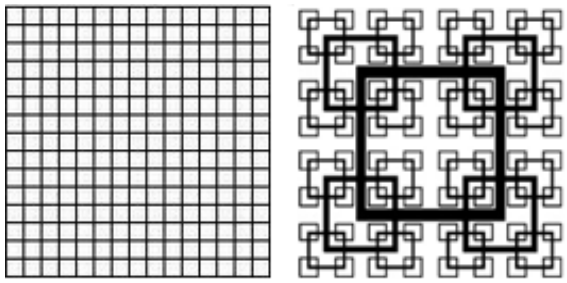

(a) (b)

Figure 2: Types of grids. (a) Classical square mesh grid and (b) fractal square grid.

The forces were measured for AOAs 0°-25° at sampling frequency of 1 kHz using two strain gauge force sensors installed at the end points of airfoil in span-wise direction; see Figure 1. The sensors measure the forces parallel and perpendicular to the wind inflow, which represent the drag and lift forces, respectively. Before measurements, the force sensors were calibrated via balances.

2.2. Analysis Approach

The measured forces are analyzed using classical averaging method and a Langevin approach. The approaches are applied on lift and drag force coefficients obtained using the relations [17]

$$C_L = \frac{F_L}{q.A} \tag{2}$$

$$C_D = \frac{F_D}{q.A} \tag{3}$$

Where F_L and F_D are the measured lift and drag forces respectively, q the dynamic pressure of wind inflow and A the airfoil area.

The classical averaging procedure is applied on C_L and C_D time series at each AOA to estimate the respective mean and standard deviation. Further, to extract more detailed information on force dynamics from this complex turbulence driven system, a Langevin approach [18] is applied in the form of drift function. The drift function in Langevin approach is a deterministic function, also known as first Kramers-Moyal coefficient, which provides full response map of local dynamics of a system. The Langevin approach based on drift function reads [19, 20, 21].

$$D(X,\alpha) = \lim_{\tau\to 0} \frac{\left(X(t+\tau) - X(t)\right)}{\tau} X(t) = X, \alpha \tag{4}$$

Where X represents the C_L or C_D, and α the fix AOA. The approach is applied directly on C_L and C_D times series at each AOA to evaluate the respective mean time derivative of C_L and C_D time series.

Additionally, for better understanding of meaning of drift function and comparison of strength in local dynamics in each grid case, a drift potential is estimated using the relation [17].

$$\phi(X,\alpha) = -\int_0^x D(\overline{X},\alpha)\, d\overline{X} \tag{5}$$

Equation (5) describes the potential in local force dynamics of a system.

3. RESULTS

The lift and drag force measurements performed in the wake of fractal and classical square grids are analyzed using the approaches described in Section 2.2. The results are presented in terms of static C_L and C_D curves with local dynamics at each AOA. Here, Figure 3 shows the results for fractal square grid, Figure 4 for 5-cm square grid and Figure 5 for 10-cm square grid. In Figures, the mean (solid line) and standard deviation (dashed lines) for C_L and C_D are obtained using classical averaging method, whereas the short-time local dynamics (red and green arrows with black crosses) by Langevin approach using Equation (4). The drift potential is achieved through Equation (5) for AOA 24° in each case. The AOA 24° represents the deep stall regime, which gives better understanding of drift potential with wide local force dynamics compared to drift potential at smaller AOAs.

Comparing the C_L results from Figures 3(a), 4(a) and 5(a), the grid with higher turbulence level (10-cm square grid) shows an increase in maximum C_L with slight shift to higher AOAs. Similar behavior was observed for measurements on NACA 634-421 airfoil by Amandolése and Széchényi [22], and on FX 79-W-151A airfoil by Schneemann et al. [17]. The C_L fluctuations in terms of standard deviation are very small in case of both classical square grids in pre-stall regime and rise gradually as stall

regime starts. In comparison to this, the standard deviations in case of fractal square grid are significantly higher in both regimes despite the lower turbulence level and lower maximum lift than the 10-cm square grid case. The short-time local C_L dynamics based on Langevin approach also show much higher fluctuations with larger potential in case of fractal square grid than both the classical square grids. The Langevin C_L curves consisting of stable fix points (black crosses where drift function is zero) of the local dynamics match almost perfectly with respective mean C_L curves in all three cases.

Again, comparing the case of C_D from Figures 3(b), 4(b) and 5(b), the grid with lower turbulence level (5-cm square grid) shows an increase in maximum C_D at higher AOAs compared to fractal and 10-cm square grid cases. However, the standard deviation in pre-stall regime is slightly lower than both the fractal and 10-cm square grids due to its low turbulence intensity. The C_D standard deviations in the wake of fractal square grid in stall regime are much higher than the classical square grids. Similarly, as in C_L case, the short-time local dynamics of C_D shows remarkable fluctuations with larger potential in case of fractal square grid compared to both classical square grids. The Langevin C_D curves consisting of stable fix points of the local dynamics have almost absolute matching with respective mean C_D curves.

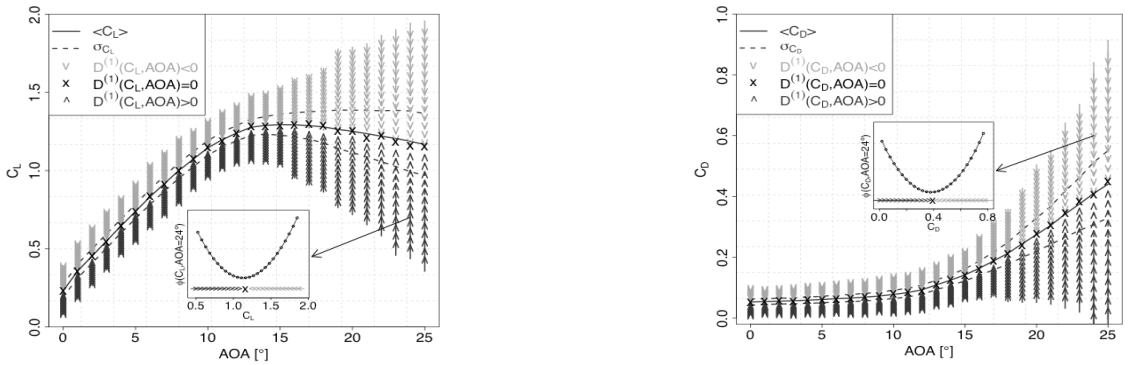

(a) (b)

Figure 3: Static C_L and C_D curves with local dynamics measured in the wake of fractal square grid. (a) C_L versus AOA, where solid blue line represents the mean C_L curve and dashed lines the standard deviation from mean. The red arrows indicate the deterministic increase in C_L and green the deterministic decrease in C_L towards the stable points; the black crosses, where drift function is zero. The black arrow points out the potential in drift function for AOA 24°. (b) C_D versus AOA and same explanation like (a) applies for (b).

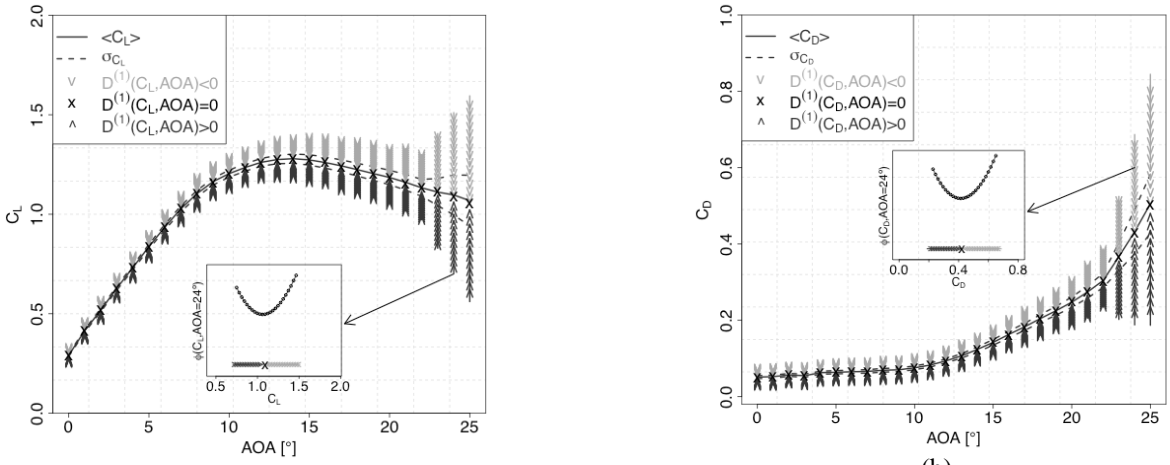

(a) (b)

Figure 4: Static C_L and C_D curves with local dynamics measured in the wake of 5-cm square mesh grid. (a) C_L versus AOA, where solid blue line represents the mean C_L curve and dashed lines the standard deviation from mean. The red arrows indicate the deterministic increase in C_L and green the deterministic decrease in C_L towards the stable points; the black crosses, where drift function is zero. The black arrow points out the potential in drift function for AOA 24°. (b) C_D versus AOA and same explanation like (a) applies for (b).

The comparison suggests that the turbulent inflow generated with fractal square grid contributes remarkable extended C_L and C_D dynamics in terms of standard deviation from the mean as well as short-time local dynamics than the classical square grids even at low turbulence intensity.

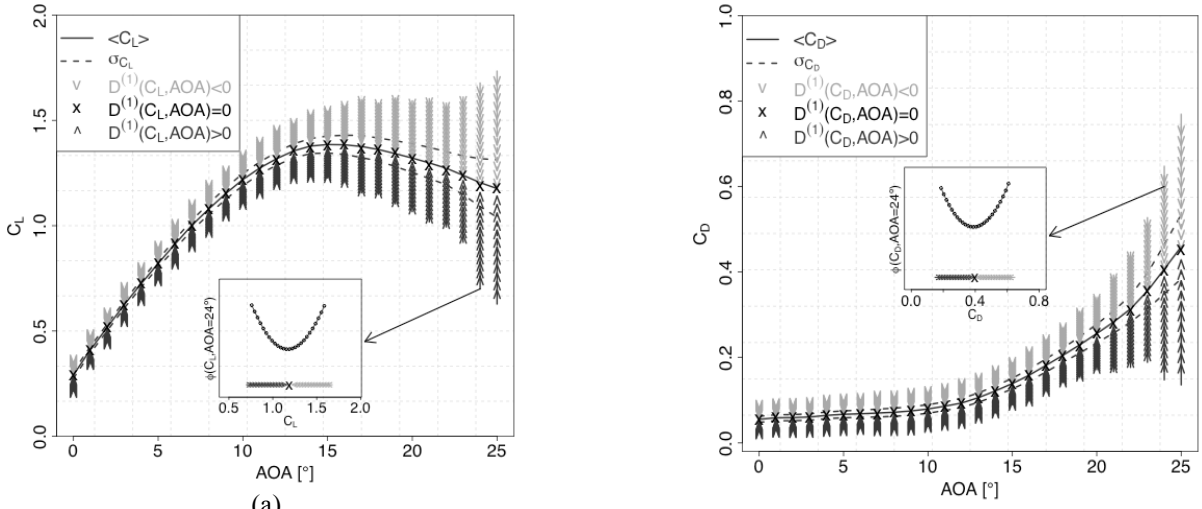

Figure 5: Static C_L and C_D curves with local dynamics measured in the wake of 10-cm square mesh grid. (a) C_L versus AOA, where solid blue line represents the mean C_L curve and dashed lines the standard deviation from mean. The red arrows indicate the deterministic increase in C_L and green the deterministic decrease in C_L towards the stable points; the black crosses, where drift function is zero. The black arrow points out the potential in drift function for AOA 24°. (b) C_D versus AOA and same explanation like (a) applies for (b).

4. CONCLUSIONS

The C_L and C_D dynamics measured in the wake of fractal and classical square grids have been analyzed using classical averaging method and a Langevin approach.

The comparison suggests that the fractal square grid wake contributes remarkable extended C_L and C_D dynamics in terms of standard deviation from the mean and short-time local dynamics extracted by Langevin approach. Even at low turbulence level, the fractal square grid wake contributes much higher force fluctuations than the classical square grids. Further, the variation of AOA has significant effect on C_L and C_D dynamics.

ACKNOWLEDGEMENTS

Authors would like to thank Jörge Schneemann for access to his measured data.

REFERENCES

[1] W. A. Timmer and R. P. J. O. M. van Rooij. Summary of the Delft University wind turbine dedicated airfoils. Journal of Solar Energy Engineering, Vol. 125, No. 4, pp. 488-496, 2003.

[2] P. Fuglsang, K. S. Dahl and I. Antoniou. Wind tunnel tests of the Risø-A1-18, Risø-A1-21 and Risø-A1-24 airfoils. Scientific report Risø-R-1112(EN), Risø National Laboratory, June 1999.

[3] P. Fuglsang, I. Antoniou, K. S. Dahl and H. A. Madsen. Wind tunnel tests of the FFA-W3-241, FFA-W3-301 and NACA 63-430 airfoils. Scientific report Risø-R-1041(EN), Risø National Laboratory, December 1998.

[4] J. Vindel, C. Yague and J. M. Redondo. Structure function analysis and intermittency in the atmospheric boundary layer. Nonlinear Processes in Geophysics, Vol. 15, pp. 915–929, 2008.

[5] N. Troldborg, J. N. Sørensen, R. Mikkelsen and N. N. Sørensen. A simple atmospheric boundary layer model applied to large eddy simulations of wind turbine wakes. Wind Energy, 2013.

[6] J. C. Kaimal and J. J. Finnigan. Atmospheric Boundary Layer Flows–Their Structure and Measurement. Oxford University Press, pp. 287, New York, 1994.

[7] B. Stoevesandt and J. Peinke. Changes in Angle of Attack on Blades in the Turbulent Wind Field. In Proceedings of the EWEC, 2009.

[8] D. M. Eggleston and F. S. Stoddard. Wind turbine engineering design. Van Nostrand Reinhold Company, New York, USA, 1987.

[9] J. G. Leishman. Principles of Helicopter aerodynamics-Cambridge Aerospace Series (2nd edn). Cambridge University Press, Cambridge, 2006.

[10] G. Wolken-Möhlmann, P. Knebel, S. Barth and J. Peinke. Dynamic lift measurements on a FX 79-W-151A airfoil via pressure distribution on the wind tunnel walls. Journal

of Physics: Conference Series, Vol. 75, No. 1, pp. 012026, 2007.

[11] G. K. Batchelor. The Theory of Homogeneous Turbulence. Cambridge University Press, Cambridge, 1953.

[12] S. Corrsin. Turbulence: Experimental methods. Handbook der Physik, Springer, New York, pp. 524, 1963.

[13] G. Comte-Bellot and S. Corrsin. The use of a contraction to improve the isotropy of grid-generated turbulence. Journal of Fluid Mechanics, Vol. 25, pp. 657, 1966.

[14] D. Hurst and J. C. Vassilicos. Scalings and decay of fractal-generated turbulence. Physics of Fluids, Vol. 19, No. 3, pp. 035103, 2007.

[15] S. Weitemeyer, N. Reinke, J. Peinke and M. Hölling. Multi-scale generation of turbulence with fractal grids and an active grid. Fluid Dynamics Research, Vol. 45, pp. 061407, 2013.

[16] M. R. Luhur, J. Peinke, J. Schneemann and M. Wächter. Stochastic modeling of lift and drag dynamics under turbulent wind inflow conditions. Wind Energy, 2014.

[17] J. Schneemann, P. Knebel, P. Milan and J. Peinke. Lift measurements in unsteady flow conditions. Scientific Proceedings of EWEC, Warsaw, Poland, 2010.

[18] H. Risken. The Fokker-Planck Equation-Edition 2. Springer, Berlin, Germany, 1996.

[19] R. Friedrich, J. Peinke and M. R. R. Tabar. Importance of Fluctuations: Complexity in the View of Stochastic Processess. Encyclopedia of Complexity and Systems Science, Springer, Berlin, Germany, 2009.

[20] A. N. Kolmogorov. Über die analytischen methoden in derwahrscheinlichkeitsrechnung. Mathematische Annalen, Vol. 104, No. 1, pp. 415-458, 1931.

[21] J. Gottschall and J. Peinke. On the definition and handling of different drift and diffusion estimates. New Journal of Physics, Vol. 10, No. 8, pp. 083034, 2008.

[22] X. Amandolése and E. Széchényi. Experimental study of the effect of turbulence on a section model blade oscillating in stall. Wind Energy, Vol. 7, pp. 267–282, 2004.